Available online at www.sciencedirect.com
ScienceDirect
Journal of the European Ceramic Society 27 (2007) 3601–3604
www.elsevier.com/locate/jeurceramsoc

Combustion synthesis and EIS characterization of TiO_2–SnO_2 system

E. Chinarro [a,*], B. Moreno [b], J.R. Jurado [a]

[a] *Instituto de Céramica y Vidrio, CSIC, C/Kelsen n 5, 28049 Cantoblanco, Madrid, Spain*
[b] *Hospital Nacional de Parapléjicos de Toledo, Finca la Peraleda s/n, Toledo, Spain*

Available online 2 April 2007

Abstract

TiO_2 is an insulator, but using specific dopants, can modify sharply its electronic structure towards semiconducting behavior. This type of response is widely applied in many electrochemical and electrocatalytical devices, namely chlorine production, hydrocarbon oxidation, CO and CO_2 hydrogenation and as electroactive substrata for biological cell growth.

Combustion synthesis is a very simple, rapid and clean method for material preparation, which will be used in the preparation of the $(1-x)TiO_2$–$xSnO_2$, $x = 0.05$–0.3. Tin oxalate and titanium isopropoxide are used as precursors for the synthesis. The as-prepared powders are fine and homogeneous, the average particle size is in the range of 5–10 nm, powders and ceramic compact bodies are characterized by DRX, SEM–TEM–EDX, DTA–TG and EIS. The impedance spectroscopy of the sample 10 mol% of SnO_2 indicates the presence of several phases which promote a matrix composite based in an electrical TiO_2 insulator compatible with an electronic conducting phase tin rich. This could be attributed to the spinodal decomposition effect observed in TiO_2–SnO_2 system.

Keywords: Powders-chemical preparation; Electrical conductivity; Impedance; TiO_2–SnO_2

1. Introduction

In the last years, there are an increasing interest in the TiO_2–SnO_2 system for its potential applications as gas sensor (H_2, CH_4, and CO),[1,2] in photocatalysis due to its important photoelectrochemical properties,[3,4] and also with the aim of controlling bacterial transport in sandy groundwater aquifers, in which metal oxides appear an alternative and provide a positively charged surface which favours cell adhesion.[5] The TiO_2–SnO_2 phase diagram exhibits a miscibility gap[6,7] thus, samples annealed inside this miscibility gap but outside the coherent spinodal decomposition can undergo phase separation by nucleation and thus, undergo precipitation. The materials proposed in this work are TiO_2-rich with a TiO_2–SnO_2 secondary phase. The preparation of thin layers of the SnO-rich phase has been published accomplish with studies on the kinetics of phase transformation in this system, carried out by Yuan and Virkar[8] and Cohen et al.[9] In these studies, the effect of aliovalent dopants on the kinetics of phase separation both inside and outside the coherent spinodal gap was examined. The rate of decomposition was drastically altered by the addition of + 3 or + 5 cations. It is well known that electrical conductivity of many ionic and electronic conductors is a sensitive function of impurities and atmosphere, but in the case of this system, it is also important to add the effect of the spinodal microstructure decomposition on their electrical properties. Chaisan et al.[7] observed that the origin of the unusual high permittivity and the non-linear current voltage behavior of this system could be due to the formation of an electrically heterogeneous structure which is derived from the spinodal decomposition. Radecka et al.[10] indicated that the chemical diffusion coefficient decreased with SnO_2 addition, the analysis of the electrical conductivity over a wide range of temperature revealed that the experimental data are in agreement with the hopping mechanism in undoped TiO_2 and band conduction in SnO_2.

Concerning the synthesis methods, the oxide mechanical mixture and the sol–gel are the most popular routes, Yang et al.[11] promoted a rapid synthesis of nanocrystalline TiO_2–SnO_2 powders, in which metal precursors were dispersed in the stearic acid at molecular level. Up to now, multicomponent oxides can be prepared by combustion synthesis.[12] In this study, the combustion synthesis of binary TiO_2–SnO_2 compositions was used. The urea is employed as fuel and the nitrates as oxidizers, sintered samples were electrically characterized by electrochemical impedance spectroscopy (EIS).

* Corresponding author. Tel.: +34 917355840; fax: +34 917355843.
E-mail address: martin@icv.csic.es (E. Chinarro).

0955-2219/$ – see front matter © 2007 Elsevier Ltd. All rights reserved.
doi:10.1016/j.jeurceramsoc.2007.02.011

2. Experimental

The TiO_2–SnO_2-based ceramics were synthesized by combustion reactions by employing Aldrich Ti (IV) isopropoxide (95%) and Sn (II) Oxalate (99%) as cation precursors. Aldrich urea, $CO(NH_2)_2$ (98%), was used as fuel. Batches were calculated on a basis of 5 g of titanium isopropoxide, being the compositions prepared $(1-x)TiO_2$–$xSnO_2$, with ($x = 0.05, 0.10, 0.15, 0.20$ and 0.30). The stoichiometric composition of each mixture was calculated based on the total oxidizing and reducing valences of the oxidizer and the fuel, in order to release the maximum energy for the reaction. The reaction produced yellow white, smooth lacy dry foams, that was easily crumbled into powder and sieved through a 100 μm mesh. The powders as-prepared were pressed into pellets and calcined up to 1450 °C during 4 h. EIS spectra was obtained (in Pt paste electroded sintered pellets of 1 cm diameter and 2 mm of thickness), by using a hot-sample holder in the temperature range of 200–900 °C employing an impedance analyzer Agilent 4294A in the frequency range of 40–10^8 Hz, the intersection with the Z'in the $-Z''$ versus Z' plot semicircles allow to determine the conductivity curves. Phase indentification of the powders and the formed disks was performed by X-ray diffraction (XRD) on a Siemens Powder Difractometer D-5000 operating at 50 kV and 30 mA using the Cu Kα radiation and Ni-filter in the range of $2\theta = 10$–70°. The scanning step was 0.05°, the time/step 1.5 s and the rotation speed used was 15 rpm. Powders morphology and microstructure was studied by scanning electron microscopy and chemical analyzed by energy-dispersive X-ray spectroscopy (SEM-EDS) with a Jeol Superprobe (JXA-8900H-WD/ED Combined microanalyzer) microscope, and by Heat Microscope with a Leitz, model Wetziar.

3. Result and discussion

The reaction produced two phases: TiO_2 and SnO_2 compatibles but not reacted, so to achieve a single phase it was necessary to calcined the combustion powders. Titanium and Tin precursors were not found as impurities in the as-prepared powders. The reaction of the whole process is described in RT:

$$SnC_2O_4\,(c) + Ti[OCH(CH_3)_2]_4 + CO(NH_2)_2\,(c) + 20.5O_2\,(g) \rightarrow SnO_2\text{–}TiO_2 + 15CO_2\,(g) + 16H_2O\,(g) + N_2\,(g) \quad (RT)$$

The combustion reaction of urea is described by the following equation:

$$CO(NH_2)_2\,(c) + 1.5O_2\,(g) \rightarrow CO_2\,(g) + 2H_2O\,(g) + N_2\,(g) \quad \Delta H^\circ = -129.9\,\text{kcal/mol} \quad (R1)$$

which is exothermic and should supply the heat needed for the synthesis reaction, during this process the ammonium nitrates should be mixed in the proportion above mentioned, to achieve the adequate conditions for combustion.

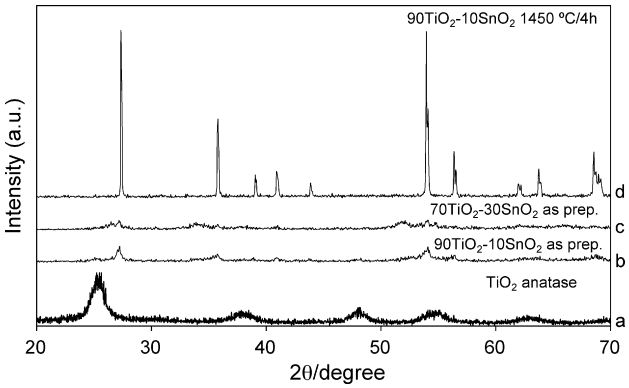

Fig. 1. XRD of (a) TiO_2; (b) $90TiO_2$–$10SnO_2$; (c) $70TiO_2$–$30SnO_2$ as-prepared powders by combustion synthesis; (d) $90TiO_2$–$10SnO_2$ sintered at 1450 °C/4 h in air.

X-ray diffraction of the as-prepared samples shows the presence and co-existence of both TiO_2 anatase and rutile phase and also SnO_2 unreacted. On the other hand, in the samples sinterized for each composition, the only reflections obtained (in the XRD pattern) were indexed as TiO_2 rutile. The Sn ions were incorporated inside the rutile lattice generating a solid solution, as it was expected by the phase diagram already described in the literature.[9] However, X-ray diffraction of the as-prepared powders treated at 1450 °C showed (Fig. 1), respectively, well crystallised TiO_2–SnO_2 (full conversion) as pure single phase. When the as-prepared powders were observed by SEM-EDX, a very fine homogeneous with sponge features is noted, and particle size is extremely small (∼15 nm), within monodal grain size distribution.

Heat microscopy measurements were done in the samples synthesized with $x = 0.10$ and 0.30, a different behavior was found when comparing both compositions. In case of $x = 0.30$ the process takes place in one step, this shrinkage observed corresponds to the TiO_2–SnO_2 rutile densification. In the case of $x = 0.10$, there are two shrinkage patterns, the first one is located at 500–600 °C and can be attributed to the presence of TiO_2 anatase or TiO_2–SnO_2 rutile phase separation, the second shrinkage step is assigned to the densification process of the TiO_2–SnO_2 rutile. The compact bodies present different densification behavior and final relative densities which are ranged between 80% and 90%. These low densities are associated to the fact that the particles synthesized by combustion exhibit a pre-sintered effect limiting the particle packing. SEM micrographs of the sintered samples (for $x = 0.1$ and 0.3) shown in Fig. 2, indicate that both microstructures are homogeneous and that the grain shape is rounded. There are significant differences between the average grain sizes (15 μm for $x = 0.1$ and 8 μm for $x = 0.3$), that fact can be explained due to the diffusion rate of tin ions into the rutile ($x = 0.1$) in the phase boundary region which is higher than in the miscibility gap, and therefore, there is a superior grain growth, as Drobeck et al.[6] proposed it their phase diagram. The latter results are in agreement with the impedance analysis of these samples.

The impedance spectra for $x = 0.05$, Fig. 3(c), contains two semicircles, the high frequency arc has an equivalent circuit with

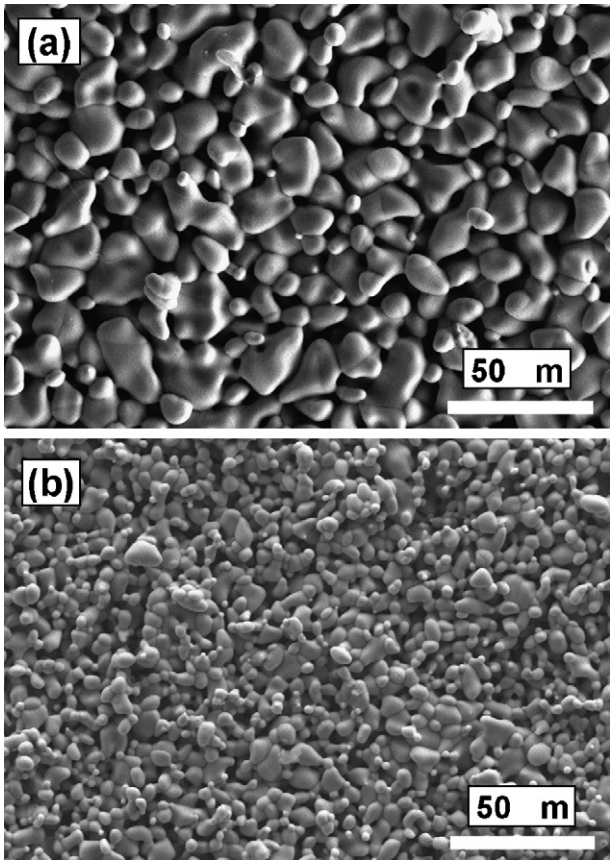

Fig. 2. SEM of (a) $90TiO_2$–$10SnO_2$; (b) $70TiO_2$–$30SnO_2$ sintered at 1450 °C/4 h in air.

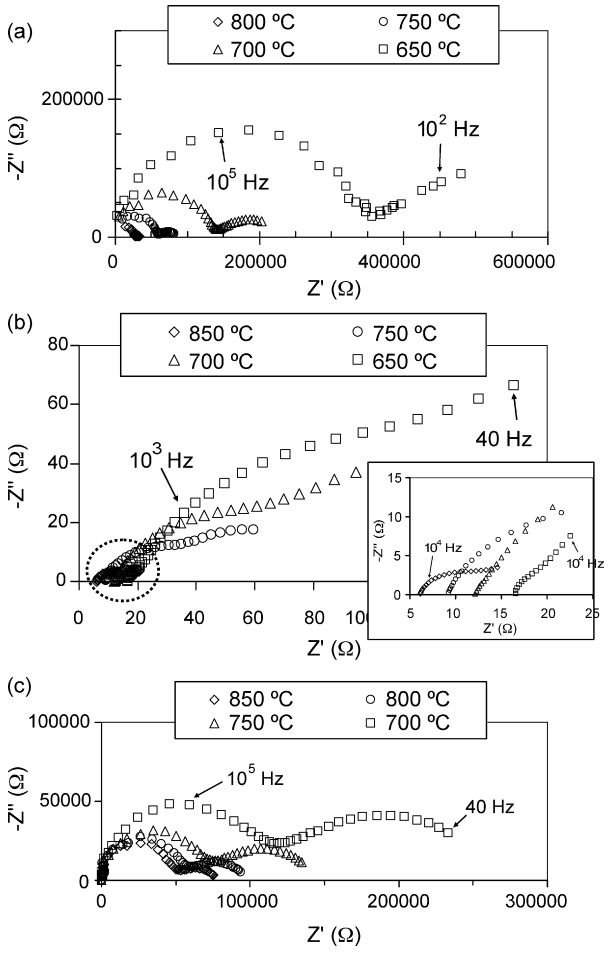

Fig. 3. EIS, from 650 to 850 °C, of the samples: (a) $70TiO_2$–$30SnO_2$; (b) $90TiO_2$–$10SnO_2$ and the amplified high frequency zone; (c) $95TiO_2$–$5SnO_2$ sintered at 1450 °C/4h in air.

a resistance in parallel with a constant phase element (CPE), and this is associated to the bulk conductivity contribution. The second one can be attributed to the presence of interfacial phases (porosity, grain boundaries and interface electrode). Those resistances obtained decrease as a function of temperature. Concerning the sample $x = 0.3$ (Fig. 3(a)), from 650 °C the arc associated with the interfacial phases was noticed by the formation of a second semicircle at low frequencies, which is similar to the spectra of $x = 0.05$.

However, for the sample $x = 0.10$, a different spectra was found (Fig. 3(b)) depending on temperature. In the range of 250–400 °C, it was found a semicircle associated to the bulk contribution and another semicircle at intermediate frequencies which can be assigned for interface contributions, grain boundary, porosity and electrode (data not shown). In the intermediate and high temperature (650–850 °C) (Fig. 3(b)) the bulk (high frequency arc) semicircles disappeared converted in a resistance, while the low frequencies dispersions observed in the spectra will become semicircles ascribed to the CPE in the interface electrode material.

The conductivity plot for total conductivity versus reciprocal temperature is depicted in Fig. 4. The plot for $x = 0.05$ (Fig. 4) from the resistance data follows an Arrhenius behavior with an activation energy of 0.71 eV, which indicates a electronic band conduction mechanism (extrinsic level is situated at 0.71 eV), similarly for $x = 0.30$ extrinsic level is situated at 1.20 eV. The conductivity plot (Fig. 4) of sample $x = 0.10$ exhibit a quite unusual pattern, because two changes in the conductivity curve are detected. The activation energies are 0.88, 0.59 and 0.42 eV from low to high temperature, these values are connected with two different electronic conduction mechanisms that can be associated: (a) to a phase-separation effect related to the TiO_2–SnO_2 rutile phase in SnO_2-rich range (high tem-

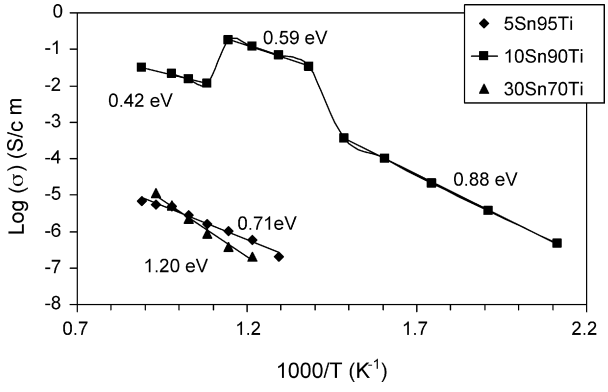

Fig. 4. Conductivity vs. 1000 T of the samples $70TiO_2$–$30SnO_2$, $90TiO_2$–$10SnO_2$ and $95TiO_2$–$5SnO_2$ sintered at 1450 °C/4 h in air, and their activation energies.

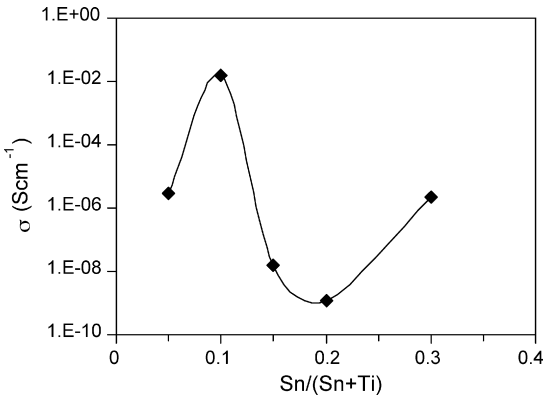

Fig. 5. Conductivity isotherm at 700 °C as a function of SnO_2 content.

perature); (b) to the TiO_2–SnO_2 rutile in TiO_2-rich phase (low temperature). Being both processes governed by band electronic conduction.

Fig. 5 depicts the conductivity isotherm at 700 °C as a function of SnO_2 content, it is observed that a maximum conductivity value is noted at $x = 0.1$, that fact is related, as it was mentioned before, to the phase boundary composition where a semiconducting phase TiO_2 rutile doped with SnO_2 governs the transport process. For $x = 0.15$ the conductivity decreases sharply and then starts to increase again at 20 mol% of SnO_2, these data are in good agreement with the work of Drobeck et al.[6] who indicated that the diffusion–precipitation is kinetically limited in the range of 15–30% of SnO_2 while from 30 mol% SnO_2 the precipitation step is energetically limited. On the contrary, Radecka et al.[10] report that in the case the composition with $x = 0.1$, in thin films, a minimum conductivity singularity was found. The only discrepancy with their results could be explained due to the synthesis route and the preparation of the samples. According to our results the spinodal decomposition is a narrow compositional effect, which means that the composition, forming and impurities fluctuation in this region can affect sharply the electronic band structure of $x = 0.1$. This fact may alter the maximum/minimum feature of this conductivity plot (Fig. 5). Besides, as Radecka et al.[10] performed their dc electrical measurements in thin films, is difficult to compare both results.

4. Conclusions

Ceramic materials from the TiO_2–SnO_2 system were achieved by using combustion synthesis. Homogeneous and pure nanocrystalline powders (15 nm) were obtained. Compact bodies exhibit quite similar microstructure behavior indicating that porosity, grain size and grain boundaries do not govern the conductivity change at $x = 0.1$. The phase boundary located at $x = 0.1$ is detected by EIS, the conductivity behavior for this composition shows two different mechanisms, the first one found in $x = 0.05$ and 0.1 is associated to a dopant effect of SnO_2 into the TiO_2 promoted a electronic band semiconductor feature. The second one, is explained by an electronic hopping process for $x = 0.3$. The EIS and conductivity behavior are correlated with the phase diagram of the SnO_2–TiO_2 system, and allow to detect a narrow spinodal decomposition effect.

Acknowledgements

Authors are grateful for the financial support from post-doctoral contracts I3P, CSIC, and APOLLON ENK5-CT-2001-00572 project. And they thank M. Carmen Fernández and Miriam Carrasco for their technical support.

References

1. Zakrzewska, K., Gas sensing mechanism of TiO_2-based thin films. *Vacuum*, 2004, **74**, 335–338.
2. Carney, C. M., Yoo, S. and Akbar, S. A., TiO_2–SnO_2 nanostructures and their H-2 sensing behaviour. *Sens. Actuators B*, 2005, **108**, 29–33.
3. Martinez, A. I., Acosta, D. R. and Cedillo, G., Effect of SnO_2 on the photocatalytical properties of TiO_2 films. *Thin Solid Film*, 2005, **490**, 118–123.
4. Pilkelton, S. and Raftery, D., Solid-state NMR studies of the adsorption and photooxidation of ethanol on mixed TiO_2–SnO_2 photocatalysts. *Solid State Nucl. Magn. Reson.*, 2003, **24**, 236–253.
5. Li, B. and Logan, B. E., Bacterial adhesion to glass and metal-oxide surfaces. *Colloids Surf. B: Biointerf.*, 2004, **36**, 81–90.
6. Drobeck, D. L., Virkar, A. V. and Cohen, R. M., The effect of aliovalent dopants on cation diffusion in TiO_2–SnO_2. *J. Phys. Chem. Solids*, 1990, **51**, 977–988.
7. Chaisan, W., Yimnirun, R., Ananta, S. and Cann, D. P., The effects of the spinodal microstructure on the electrical properties of TiO_2–SnO_2 ceramics. *J. Solid State Chem.*, 2005, **178**, 613–620.
8. Yuan, T. C. and Virkar, A. V., Kinetics of spinodal decomposition in the TiO_2–SnO_2 system—the effect of aliovalent dopants. *J. Am. Ceram. Soc.*, 1988, **71**, 12–21.
9. Cohen, R. M., Drobeck, D. L. and Virkar, A. V., *J. Am. Ceram. Soc.*, 1988, **71**, 401.
10. Radecka, M., Pasierb, P., Zakrzewska, K. and Rekas, M., Transport properties of (Sn,Ti)O_2 polycrystalline ceramics and thin films. *Solid State Ionics*, 1999, **119**, 43–48.
11. Yang, J., Li, D., Wang, X., Yang, X. and Lu, L., Rapid synthesis of nanocrystalline TiO_2/SnO_2 binary oxides and their photoinduced decomposition of methyl orange. *J. Solid State Chem.*, 2002, **165**, 193–198.
12. Chinarro, E., Moreno, B., Martín, D., González, L., Villanueva, E., Guinea, D. and Jurado, J. R., Posibilidades del análisis de imagen para el estudio de la síntesis de materiales por combustión. *Bol. Soc. Esp. Ceram. Vidrio*, 2005, **44**, 105–112.